NASA/TM–2017–219602

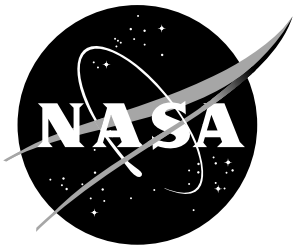

CFD Study of NACA 0018 Airfoil with Flow Control

Christopher A. Eggert
Purdue University, West Lafayette, Indiana

Christopher L. Rumsey
Langley Research Center, Hampton, Virginia

April 2017

NASA STI Program. . . in Profile

Since its founding, NASA has been dedicated to the advancement of aeronautics and space science. The NASA scientific and technical information (STI) program plays a key part in helping NASA maintain this important role.

The NASA STI Program operates under the auspices of the Agency Chief Information Officer. It collects, organizes, provides for archiving, and disseminates NASA's STI. The NASA STI Program provides access to the NASA Aeronautics and Space Database and its public interface, the NASA Technical Report Server, thus providing one of the largest collection of aeronautical and space science STI in the world. Results are published in both non-NASA channels and by NASA in the NASA STI Report Series, which includes the following report types:

- TECHNICAL PUBLICATION. Reports of completed research or a major significant phase of research that present the results of NASA programs and include extensive data or theoretical analysis. Includes compilations of significant scientific and technical data and information deemed to be of continuing reference value. NASA counterpart of peer-reviewed formal professional papers, but having less stringent limitations on manuscript length and extent of graphic presentations.
- TECHNICAL MEMORANDUM. Scientific and technical findings that are preliminary or of specialized interest, e.g., quick release reports, working papers, and bibliographies that contain minimal annotation. Does not contain extensive analysis.
- CONTRACTOR REPORT. Scientific and technical findings by NASA-sponsored contractors and grantees.
- CONFERENCE PUBLICATION. Collected papers from scientific and technical conferences, symposia, seminars, or other meetings sponsored or co-sponsored by NASA.
- SPECIAL PUBLICATION. Scientific, technical, or historical information from NASA programs, projects, and missions, often concerned with subjects having substantial public interest.
- TECHNICAL TRANSLATION. English-language translations of foreign scientific and technical material pertinent to NASA's mission.

Specialized services also include organizing and publishing research results, distributing specialized research announcements and feeds, providing information desk and personal search support, and enabling data exchange services.

For more information about the NASA STI Program, see the following:

- Access the NASA STI program home page at `http://www.sti.nasa.gov`
- E-mail your question to `help@sti.nasa.gov`
- Phone the NASA STI Information Desk at 757-864-9658
- Write to:
  NASA STI Information Desk
  Mail Stop 148
  NASA Langley Research Center
  Hampton, VA 23681-2199

NASA/TM–2017–219602

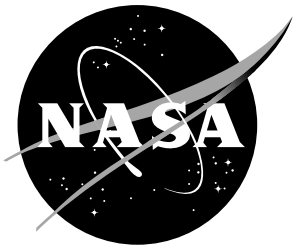

CFD Study of NACA 0018 Airfoil with Flow Control

Christopher A. Eggert
Purdue University, West Lafayette, Indiana

Christopher L. Rumsey
Langley Research Center, Hampton, Virginia

National Aeronautics and
Space Administration

Langley Research Center
Hampton, Virginia 23681-2199

April 2017

Acknowledgments

The authors acknowledge the help of David Greenblatt and Hanns Muller-Vahl of the Technion-Israel Institute of Technology, who conducted the experiment associated with this study. The experiment and subsequent collaboration was supported in part by the United States - Israel Binational Science Foundation.

Available from:

NASA STI Program / Mail Stop 148
NASA Langley Research Center
Hampton, VA 23681-2199
Fax: 757-864-6500

Abstract

The abilities of two different Reynolds-Averaged Navier-Stokes codes to predict the effects of an active flow control device are evaluated. The flow control device consists of a blowing slot located on the upper surface of an NACA 0018 airfoil, near the leading edge. A second blowing slot present on the airfoil near mid-chord is not evaluated here. Experimental results from a wind tunnel test show that a slot blowing with high momentum coefficient will increase the lift of the airfoil (compared to no blowing) and delay flow separation. A slot with low momentum coefficient will decrease the lift and induce separation even at low angles of attack. Two codes, CFL3D and FUN3D, are used in two-dimensional computations along with several different turbulence models. Two of these produced reasonable results for this flow, when run fully turbulent. A more advanced transition model failed to predict reasonable results, but warrants further study using different inputs. Including inviscid upper and lower tunnel walls in the simulations was found to be important in obtaining pressure distributions and lift coefficients that best matched experimental data. A limited number of three-dimensional computations were also performed.

1 Introduction

Blowing slots have long been pursued as a means of controlling the forces generated by a wing, often by injecting momentum with the goal of reducing or eliminating separation. There are numerous uses for such a technology, such as for high-lift systems or low-drag control surfaces on aircraft. At Technion Israel Institute of Technology, Greenblatt [1] has recently been investigating the use of an unsteady low-speed wind tunnel to explore blowing effects for airfoils that are dynamically pitching. This type of problem represents a challenge for CFD, both because of the highly unsteady nature of the flow as well as because of known limitations of Reynolds-averaged Navier-Stokes (RANS) for computing separated flows. More advanced CFD methods such as large-eddy simulation (LES) are still considered too expensive for routine use.

The particular experiment that provided the comparison data [2] for this study was performed with the intent of improving the performance of wind turbines. One major challenge in the design of wind turbines is the harmful effect of unsteady loads on the blades. This type of active flow control could be used to reduce these unsteady loads by increasing or reducing the lift generated as the turbine blade cycles, as well as by reducing or eliminating dynamic stall.

This experiment has several characteristics that often challenge CFD codes. First, the Reynolds numbers were relatively low (less than 400,000 based on airfoil chord). Such low Reynolds numbers means that the flow is transitional. Transitional flows generally pose problems for standard turbulence models, which are intended for fully turbulent situations. The experiment also experiences three-dimensional effects where the airfoil intersects the tunnel sidewalls. Because the tunnel width-to-chord ratio is relatively low (approximately 1.75), these three-dimensional effects likely occur over a significant fraction of the model at high angles of attack; and 2-D computations would be questionable at such conditions. Finally, the upper and lower wind tunnel walls are only $1.44c$ above and below the airfoil. The wall presence is therefore likely very influential on the flowfield near the airfoil. For

CFD, this in and of itself is not a big problem, but it does require the generation of a new grid for every angle of attack. And for dynamic stall investigations, an overset or deforming grid would be required.

In this study, we investigate the effect of code, turbulence model, and grid on two cases with blowing from the leading edge slot (in addition to the baseline case of no blowing). We also investigate the influence of the wind tunnel walls and the relative importance of three-dimensionality. Although the experiment was primarily concerned with dynamic stall [2,3], here we focus the CFD study primarily on the effect of flow control (steady blowing) at steady-state conditions and at angles of attack mostly below or near stall.

2 Geometry and Flow Characteristics

The wind tunnel experiment from which the results were obtained tested an NACA 0018 airfoil model with two blowing slots cut into the upper surface, located at 5 and 50% of the chord (see figure 1(a)). These slots point at a 20 degree angle toward the trailing edge of the airfoil. The airfoil model had span $b = 0.610$ m and chord length $c = 0.347$ m, and was placed in a wind tunnel with dimensions 0.610 m wide $\times$ 1.004 m high (see figure 1(b)). In the experiments chosen for comparison, $Re_c = 250,000$ and freestream $M = 0.03265$ ($U_\infty = 11.1$ m/s).

There were 40 pressure taps along the upper and lower surfaces of the model to provide the experimental pressure coefficient C_p values, which were then used to calculate the experimental values of the lift coefficient C_L.

The geometry used in the CFD trials varied slightly from the experimental geometry. The slot height of the as-designed model was originally specified as 1 mm. However, the model, once manufactured, had a slot height of 1.2 mm. In this study, because there was no computer-aided design (CAD) representation for the as-built slots, the original specified slot height of 1 mm was used in the construction of all grids. However, the momentum coefficient C_μ, defined by

$$C_\mu = \frac{hU_j^2}{(1/2)cU_\infty^2} \tag{1}$$

which is a measure of the effect of blowing, was kept consistent between CFD and experiment. Previous experiments [4] showed that when $h << c$, the measured results of blowing depend only on C_μ, and are not sensitive to changes in h. In Eq. (1), h is the slot height, U_j is the jet blowing velocity, c is the airfoil chord, and U_∞ is the freestream velocity.

3 CFD Codes and Turbulence Models

Two NASA CFD codes were used in this study: CFL3D and FUN3D. Both codes solve the RANS equations.

CFL3D [5] is a structured-grid upwind multi-zone CFD code that solves the generalized thin-layer or full Navier-Stokes equations. In the current study, the full viscous terms are used for all computations. CFL3D can use point-matched, patched, or overset grids and employs local time-step scaling, grid sequencing and multigrid to accelerate convergence

to steady state. CFL3D is a cell-centered finite-volume method. It uses third-order upwind-biased spatial differencing on the convective and pressure terms, and second-order differencing on the viscous terms; it is globally second-order accurate. Roe's flux difference-splitting method [6] is used to obtain fluxes at the cell faces. The solution is advanced in time with an implicit approximate factorization method. For each loosely coupled iteration, the mean flow equations are advanced in time with the eddy-viscosity fixed; then the turbulence model is advanced in time with the mean flow solution fixed. Several turbulence models are available in the code, including the one-equation model of Spalart-Allmaras [7] (SA), the two-equation shear stress transport (SST) model of Menter [8], and the four-equation γ-Re_θ SST transition model of Langtry-Menter [9]. These models are not described here; see the Turbulence Modeling Resource website [10] or the original references for complete descriptions.

FUN3D [11, 12] is a finite-volume solver in which the flow variables are stored at the vertices or nodes of the mesh. FUN3D solves the equations on mixed element grids, including tetrahedra, pyramids, prisms and hexahedra. The code also has a two-dimensional path for triangular and quadrilateral grids. At interfaces between neighboring control volumes, the inviscid fluxes are computed using an approximate Riemann solver based on the values on either side of the interface. Several convective flux schemes are available in FUN3D. The most common scheme for subsonic and transonic flows is Roe's flux difference splitting, [6] which is used in the current study. For second-order accuracy, interface values are obtained by extrapolation of the control volume centroidal values, based on gradients computed at the mesh vertices using an unweighted least-squares technique. Several reconstruction limiters are available in FUN3D, but none were used in this study. The solution at each time-step is updated with a backwards Euler time-integration scheme. At each time step, the linear system of equations is approximately solved with either a multi-color point-implicit procedure or an implicit-line relaxation scheme [13]. Local time-step scaling is employed to accelerate convergence to steady state. The same turbulence models mentioned for CFL3D (SA, SST, and γ-Re_θ) are also available in FUN3D.

4 Grid Characteristics and CFD Boundary Conditions

A series of grids was used to identify the effectiveness of each code and turbulence model. All grids were produced in Pointwise®, a commercial grid generator capable of creating both structured and unstructured grids.

First, a 2-D, structured, free-air grid was used with both codes (CFL3D and FUN3D) to verify that they produced similar results. This grid was also used to perform an initial grid sensitivity study, the results of which were consulted during the creation of other structured and unstructured grids in the series. These initial structured grids used a sharp trailing edge on the airfoil. The finest grid size had $687,093$ grid points (per plane), or $684,032$ grid cells, and 1073 grid points on the airfoil surface, with minimum spacing of $2.88 \times 10^{-6}c$ of the first grid point off the wall and farfield extent of $144c$ (chord length c was 0.347 m). Each successively coarser level was created by removing every other grid point in each coordinate direction from the next finer grid. The minimum wall spacing of the finest grid ensured that the Δy^+ spacing of the first grid point off the wall was less than 1 for all grid levels. Inside the airfoil slots, the walls were treated inviscidly, so inviscid wall spacing was

used (approximately in the range of $0.0001c - 0.001c$). A view of the structured free-air grid is shown in figure 2(a) and (b). Adiabatic no slip boundary conditions were applied on the airfoil, except within the slots, whose side walls were treated as slip surfaces. When blowing was used, density and velocity were specified at the lower wall of the slot's plenum, while pressure was extracted from the interior of the domain (density was set to freestream, and velocity was set in an iterative fashion to achieve the correct average velocity near the slot exit). When blowing was not used, the lower wall of the slot's plenum was treated as a slip surface. At the outer boundary of the grid, a farfield Riemann-invariant boundary condition was employed.

A series of 2-D structured grids incorporating inviscid upper and lower tunnel walls was then created to identify the effect that the walls' presence had on the lift coefficient and pressure distribution along the airfoil. A different grid was created for each angle of attack investigated (see, for example, figure 2(c)). These grids also used a sharp trailing edge on the airfoil. The grid used here was based on the finest grid level from the free-air grid convergence study. Its size was $407,523$ grid points (per plane), with 1073 grid points on the airfoil surface and minimum spacing of $2.88 \times 10^{-6}c$ of the first grid point off the wall. The tunnel walls extended from $5.76c$ in front of the airfoil quarter chord to $5.76c$ behind it. Normal grid spacing at the tunnel walls (treated inviscidly) was approximately in the range of $0.01c - 0.06c$. Inside the airfoil slots, the walls were again treated inviscidly. For these grids, the boundary conditions on the airfoil surface and within its slots were the same as before. The upper and lower tunnel walls were treated as slip surfaces. At tunnel inflow, the total pressure and total temperature were specified according to adiabatic relations using $M = 0.03265$: $p_t/p_{ref} = 1.00075$, $T_t/T_{ref} = 1.00021$, and Riemann invariants were extrapolated from the interior of the domain. At tunnel outflow, static pressure was specified as $p/p_{ref} = 1.0$, and all other quantities were extrapolated from the interior.

A series of 2-D unstructured grids (with triangular elements) incorporating inviscid upper and lower tunnel walls was also created. A different grid was created for each angle of attack investigated (see, for example, figure 2(d)). To explore the influence of airfoil trailing edge shape, these grids also used a blunt trailing edge on the airfoil, approximately corresponding to the actual bluntness of the wind tunnel model (about $0.0035c$ thickness). Although details are not provided in this report, the influence of the modeled trailing edge thickness was found to be insignificant in terms of the results of interest (surface pressure coefficients and lift coefficients) for this study. These grids contained $384,732$ grid points (in the 2-D plane), and used 2141 grid points on the airfoil surface and minimum spacing of $2.88 \times 10^{-6}c$ of the first grid point off the wall. Tunnel wall extent was somewhat different from the structured tunnel grids, with the downstream end extending to $8.64c$. Normal grid spacing at the tunnel walls (treated inviscidly) was approximately $0.007c$. Boundary conditions for these grids were the same as for the structured tunnel grids, except that the side walls inside the airfoil slots were treated viscously (the grids had finer spacing and the boundary conditions were adiabatic no-slip). This viscous slot treatment was done to overcome a problem running FUN3D with some of the turbulence models.

A few runs were also performed in 3-D. For these, the 2-D, structured, tunnel grid was extruded in the spanwise (y) direction a distance of $y = 0.305$ m, representing the tunnel half width. Grids spacing was clustered near $y = 0$, representing the tunnel side wall. See figure 2(e).

The grids used in this study each included the contracting portion of the blowing slots

between the slot plenums and the actual slot exit, as shown in figure 2(b). Therefore, the boundary condition at the plenum exit was set as a subsonic inflow when the slot was blowing. The inflow velocity at this boundary was adjusted so that the jet velocity U_j (velocity at the slot exit line) matched the correct value for the chosen case. The target jet velocities were found by rewriting Eq. (1) as

$$U_j = \sqrt{\frac{(1/2)C_\mu c U_\infty^2}{h}} \tag{2}$$

then solving Eq. (2) for U_j using each value of C_μ included in the study. The target jet velocity is equal to 32.693 m/s when C_μ = 5%, and 11.325 m/s when C_μ = 0.6%. When nondimensionalized with the reference speed of sound, these two velocities are 0.096155 and 0.03331, respectively.

To ensure that the jet velocity matched the target velocities for each value of C_μ, an iterative process was used in which the average velocity of the CFD solution across the slot exit line was found, then adjustments were made to the plenum inflow boundary condition until the desired average jet velocity was attained (see figure 3). The inflow boundary condition required was approximately the same regardless of whether the interior slot walls were treated inviscidly or viscously.

5 Results

The results include grid sensitivity studies (both grid density as well as comparison of results with structured and unstructured grids). Comparisons are made using different codes and different turbulence models. Efforts to model or capture transitional effects are described, and the effects of including the tunnel upper and lower walls are documented. Most computations are 2-D, but several 3-D trials were also explored (i.e., including tunnel side walls).

5.1 Structured Grid Sensitivity Studies

A grid sensitivity study was performed on the 2-D, structured, free-air grid. The original "fine" grid ($684,032$ cells) was coarsened by removing every other grid point to produce a "medium" grid ($171,008$ cells), then coarsened again to produce a "coarse" grid ($42,752$ cells). For the purposes of the grid sensitivity study, the case was run at several angles of attack without blowing. Lift coefficient results are plotted in figure 4. The results indicated little influence of grid density on lift coefficients over the angle of attack range of interest, so the medium grid was selected for use in obtaining further "free-air" results.

Notice in figure 4 that the experiment yielded an unusual lift curve shape. Rather than an approximately linear progression of lift with angle of attack over the lower angles, the experimental results exhibited a nonlinear increase in lift between approximately 5 and 10 degrees. This is believed to be due to the presence of a laminar bubble near the airfoil's upper surface leading edge, which causes additional flow acceleration around it. As will be described further below, the CFD was not able to capture this effect.

5.2 Code Comparison

Several test cases were run in both CFL3D and FUN3D to identify whether the two codes would produce similar results for this case. The angles of attack used were 0, 5, 8, 10, and 12 degrees. A sample of these results can be found in figure 5. These results show that on the same sufficiently refined grid for this case, CFL3D and FUN3D produce practically identical solutions.

5.3 Turbulence Model Comparison

Next, three turbulence models were examined using the same test cases. The results of these runs can be found in figures 6 and 7. The SA and SST models displayed similar behavior of relatively linear lift curve slope (failing to predict the nonlinear change in the lift curve slope between 5 and 10 degrees angle of attack). However, their pressure distributions were reasonable and consistent with each other and with the experiment.

The γ-Re_θ turbulence model was used to attempt to capture the nonlinear lift curve behavior. C_L results at $\alpha = 5^\circ$ appeared to be promising. The model yielded delay of transition to turbulence on the upper surface, resulting in a series of small recirculating regions on the upper surface, which were products of a very large region of separated laminar flow. Example plots showing the extent of these regions can be seen in figure 7(b), (d), and (f). However, the experiment showed that laminar separation bubble reattachment occurred prior to 0.07 m along the chord in all cases for which the forward inactive slot on the upper surface tripped the flow to turbulent [2]. Such large separated regions from the γ-Re_θ model indicated its failure to capture the tripping effect of this slot.

The cause of the failure of the γ-Re_θ model has not been determined, but one potential cause is the natural decay of freestream turbulence intensity inherent in the model. Turbulence intensity was specified to be 0.05%, based on information provided by the experimenters. A large portion of that intensity might have decayed over the length of the grid, so that the level near the airfoil was too low for the model to accurately predict transition. Future efforts should focus on either adjusting the freestream turbulent boundary conditions or disallowing their decay; also, time-accurate computations may be required with this model to find the average of any inherent unsteadiness due to laminar separation. However, this model was not pursued further in the current study.

5.4 Forced Transition Study

To investigate the effects that transition location might have on the flow solutions, several test cases were run in which the transition location was specified in conjunction with the SA model. The ultimate goal of these particular runs was to determine if transition location could alter the solution enough to produce the behavior in the lift curve slope similar to that seen in the experimental data. Transition effects were one of the first suspected causes of the behavior, since CFD is generally unreliable at predicting transition characteristics at low Reynolds numbers such as the one in this problem. Seven transition locations on the upper surface of the airfoil were tested, ranging from approximately 5% (the location of the blowing slot) to 25% of chord length. Results from these tests can be found in figures 8 and 9.

There were only small changes in the lift curve as the transition location varied (figure 8). Looking at the solutions in more detail, as the laminar region increased in size, a small region of lower pressure was observed in the solution on the upper surface (the growing "hump" in the pressure distributions in figures 9(a) and (b)). Additionally, the flow solution developed regions of recirculation if the transition was delayed far enough. See, for example, figure 9(d), in which the skin friction goes negative for transition locations aft of approximately $x/c = 0.07$. However, these CFD trends do not appear to be matching the experimental data very well. Also, even though the lift coefficients increased slightly as transition location was moved aft, the C_L values from CFD never approached the levels seen in the experimental data between $5^\circ < \alpha < 10^\circ$.

This particular 2-D test failed to identify the cause of the nonlinearity in the experimental lift curve. Therefore, the remainder of the CFD cases were run fully turbulent. Attempts to capture the nonlinearity were abandoned in order to focus on the larger effects of the blowing slot on the lift curve.

5.5 Two-Dimensional Structured Grid Results

The first results to display the effects of slot blowing can be found in figure 10. These results were obtained from FUN3D runs on the 2-D, structured, free-air grid. The lift coefficient results clearly exhibit the same trends as the experimental data, and are fairly accurate at lower angles of attack. However, the CFD failed to capture details such as the reduced stall angle of attack in the $C_\mu = 0.6\%$ case.

The pressure distributions in figure 11 also match fairly well with the experimental data for most cases. The main difference between CFD and experiment is that CFD tends to predict higher pressure on the upper surface than is found in the experiment. For cases in which massive separation is present in the flow, such as in figure 11(c), the pressure distributions do not match well at all. This was expected, since RANS CFD generally fails to model massively separated flows correctly.

5.6 Structured Free-Air vs. Tunnel Grid Computations

New grids were created to examine the effect that upper and lower tunnel walls have on the flow solution. First, a structured tunnel grid was created (more details on grid construction are found in Section 4). The results from this grid are compared to those from the free-air grid in figures 12 and 13. This comparison shows that including the tunnel walls greatly improved correlation between the CFD solutions and the experimental results. Both lift coefficient results and surface pressures better match the experimental data. For this reason, upper and lower tunnel walls were determined to be a necessary inclusion in all subsequent computations.

5.7 Two-Dimensional Unstructured Grid Results

Unfortunately, an undiagnosed issue within FUN3D caused the SST turbulence model to fail to produce a solution on the 2-D structured tunnel grid for all test cases. In an attempt to remedy this problem, an unstructured tunnel grid with viscous slot walls (but with otherwise similar characteristics as the 2-D structured tunnel grid) was created and tested. Both SA

and SST turbulence models produced useful results with this new grid. Overall, the effects of slot blowing were captured very well in these CFD trials, as shown in figures 14 and 15. At lower angles of attack, the changes in lift coefficient caused by the blowing were matched extremely well. At higher angles of attack, the CFD missed absolute levels but appeared to generally capture the trends with different blowing coefficients.

Unlike the results from the structured free-air grid shown in figure 10, these CFD trials captured the stall behavior of the airfoil for all three momentum coefficients: stall was delayed past the tested range of angles when $C_\mu = 5\%$, stall began around $\alpha = 15^\circ$ when no slot blowing is used, and stall was induced early at around $\alpha = 9^\circ$ when $C_\mu = 0.6\%$. However, despite the fact that the start of stall behavior was correctly predicted, CFD performance deteriorated beyond stall (massive separation). As expected for these cases, CFD typically did not converge to steady-state results. The error bars in figure 14 represent the amplitude with which the CFD solutions oscillated about the mean values at their most converged states. Because of this nonconvergence, time-accurate runs were required (as described later). Comparisons of pressure coefficients (figure 15) were generally excellent for both SA and SST, with the exception of the stalled high angle of attack case with $C_\mu = 0.6\%$, shown in figure 15(f).

Figure 16 shows typical residual and lift histories for these cases, for FUN3D using the SA model. In the unstructured tunnel grid at $\alpha = 12.5^\circ$, when $C_\mu = 5\%$, residuals were driven to machine zero and lift was well converged. But when $C_\mu = 0$ or 0.6%, the code did not converge at this angle of attack: residuals were nonconvergent and the lift oscillated.

Prior to continuing with runs on the 2-D unstructured tunnel grids, a grid study analysis was performed. FUN3D was run with the airfoil at $\alpha = 10^\circ$ on several grid levels of both the 2-D structured and unstructured tunnel grids. Lift coefficient results are plotted in figure 17. In this plot, h_g represents a measure of the average overall grid spacing. An infinite grid is approached as $h_g \to 0$. From this plot, it is clear that the solutions on unstructured triangle grids are more grid-sensitive than solutions on the structured grid. For a given number of unknowns, the structured grid solution yields a result that is closer to the grid-converged result. However, both grid types approach approximately the same result, as expected. Based on this result, the unstructured grid with $h_g \approx 0.0015$ appears to provide C_L results that are within about 5% of the grid converged solution. This unstructured grid level was considered to be adequate for this study.

To further explore the nonconvergent (oscillating) solutions, all $C_\mu = 0.6\%$ cases were run again, time-accurately, in FUN3D. These cases had large amounts of separation at high angles of attack, so they were used to identify the effects of running time-accurately on the CFD results. Results from the time-accurate trials, presented in figure 18 alongside the steady results, showed that the solution oscillations could be reduced dramatically with time-accurate computations. Although the error bars, which represent the amplitude of the solution oscillation, were much smaller for the time-accurate solutions, generally the overall trends in the lift behavior were similar to the steady-state runs. Although not shown, the C_p results for time-accurate runs were similar; i.e., still in reasonable agreement with experiment except for stalled high angle of attack cases with $C_\mu = 0.6\%$.

Current results using FUN3D and the SST model are compared to independent SST results using a different CFD code (Laufer [14]) in figure 19. The two codes used independently-generated grids, both including tunnel top and bottom walls. Laufer's grids did not include internal plenums, but rather imposed blowing boundary conditions at the "slot exit" loca-

tion. Generally, the results from the two codes are in very close agreement. Note that, like FUN3D, Laufer's CFD results also missed the nonlinear behavior in the lift curve slopes, believed to be caused by the presence of a laminar bubble in the experiment.

Figure 20 shows the general effect of the blowing on the trailing edge separation location (in this case for FUN3D using the SA turbulence model). For no blowing, the airfoil at zero degrees angle of attack has no trailing edge separation, but separation appears as the angle of attack is increased. For example, at $\alpha = 10^\circ$, separation occurs at approximately $x/c = 0.72$. With weak blowing at $C_\mu = 0.6\%$, the trailing edge separation is more pronounced (at $\alpha = 10^\circ$, separation occurs ar approximately $x/c = 0.51$). On the other hand, strong blowing at $C_\mu = 5.0\%$ has a Coanda effect and delays the presence of any trailing edge separation until beyond $\alpha = 10^\circ$. Even as high as $\alpha = 15^\circ$, separation is still near the trailing edge ($x/c = 0.86$).

A comparison of experimental (PIV) and CFD velocity fields can be found in figure 21, for $\alpha = 15^\circ$. Detailed flow features could not be quantitatively matched, but as can be seen from the size of the recirculating regions, the CFD flow solutions were qualitatively capturing the trends. Running time-accurately did not substantially improve the RANS results.

5.8 Preliminary Three-Dimensional Computations

A limited number of 3-D trials were conducted to identify whether 3-D effects could have had a significant impact on the experimental pressure data. The grid for these trials was originally intended to be the 2-D unstructured grid, extruded approximately 80 times in the spanwise direction. However, 3-D runs in FUN3D failed to produce reasonable results on this grid (due to a bug that was discovered, diagnosed, and fixed well after the current study was completed).

For this reason, the structured 2-D grid was selected instead as the basis for the 3-D grid. This 2-D grid was extruded 81 times in the spanwise direction The spanwise spacing near one side of the grid had viscous spacing (representing the wind tunnel side wall), while the other side had coarser spacing (representing the center of the wing section). This grid was used in both CFL3D and FUN3D.

Visualizations of the 3-D effects when the wing is at $\alpha = 12.5^\circ$ can be found in figure 22. Here, in all blowing cases, corner effects create a large area of recirculation on the upper surface of the airfoil. At $\alpha = 12.5^\circ$, CFL3D results with no blowing in figure 22(a) shows significant trailing edge separation across the entire wing span, along with a large corner separation region near the side wall. With $C_\mu = 5\%$ blowing (figure 22(b)), most of the wing is attached, but there is still a significant region of corner separation. Finally, with $C_\mu = 0.6\%$ (figure 22(c)), the entire wing is massively separated, and isolating the effects of trailing edge separation and corner separation is difficult.

It is known that linear turbulence models can sometimes overpredict the size or influence of corner separation [15, 16]. One known fix for this is the Quadratic Constitutive Relation (QCR2000) of Spalart [17]. In FUN3D, 3-D cases at a low angle of attack of $\alpha = 5^\circ$ were run with the SA model as well as with the SA-RC-QCR2000 model (where "RC" indicates an additional Rotation-Curvature correction [18]). Results are shown in figure 23. For this case, the corner separation was relatively small, and the inclusion of RC and QCR2000 made little perceptible difference.

To investigate how much these 3-D effects have an impact on the pressure distribution along the center of the wing section, which is where the pressure taps were located during the experiment, the pressure distributions along the wing centerline were plotted in figure 24 for the same $\alpha = 5^\circ$ case. From this zoomed-in plot, CFL3D and FUN3D are seen to produce similar 3-D results (as well as similar 2-D results), with the 2-D and 3-D results showing some difference from each other. The 2-D results yielded somewhat lower C_p levels on both the lower and upper surfaces, and tended to agree better with the experimental data than the 3-D computations. This plot indicates that even small 3-D effects in the solution near the wall have some influence on the "two-dimensional" region near the tunnel center plane. This same conclusion was reached in an earlier study on a high-lift airfoil. [19] Simply stated, there is really no such thing as a "two-dimensional" experiment: any three-dimensionality present near side walls will affect to some degree the region of the flow that is presumed to be nominally two dimensional.

Another interesting preliminary result from the 3-D trials can be seen in figure 25, which plots FUN3D results at $\alpha = 12.5^\circ$ (using the SA-RC-QCR2000 model on the structured 3-D grid, no blowing). Figure 25(a) shows surface streamlines and surface pressure coefficient contours, indicating the three-dimensional nature of this solution. Nonetheless, the C_p cuts along the span (shown in figure 25(b)) are relatively uniform, ranging from near the wall located at $y = 0$ m to the center plane located at $y = 0.305$ m. All cuts consistently underpredict the negative peak C_p near the nose. However, the pressure distribution immediately aft of the blowing slot clearly changes across the span of the wing section. This indicates that a separated region exists behind the slot near the tunnel center plane, but not near the wall. The effect appears to mimic the experimental data (taken along the tunnel centerplane). 2-D CFD solutions for this case (not shown) did not indicate separated flow behind the slot. This 3-D solution again illustrates the highly three-dimensional nature of this experiment, calling into question the use of 2-D CFD to try to compute this flow, for anything other than qualitative analysis.

6 Conclusions

RANS computations of an NACA 0018 airfoil (with and without leading edge blowing) were investigated. The independent codes CFL3D and FUN3D were confirmed to yield very close results when run on the same structured grid. Of the three turbulence models tested, only the SA and SST models produced useful results in this study. These two models, run fully turbulent, predicted qualitative flow characteristics consistent with those present in the experimental data for most test cases, although neither was able to predict the nonlinear behavior of the experimental lift curve (believed to be caused by transitional effects). SA and SST were also fairly consistent with each other on all test cases. SA generally predicted slightly higher values of C_L than SST, and the pressure and skin friction distributions showed little difference. The γ-Re_θ transition model predicted laminar regions that were too large, and therefore failed to produce reasonable results. However, it may yet prove to be applicable to this blowing slot problem if adjustments are made to its freestream boundary conditions. A forced transition study was also attempted, but it could not predict the nonlinear behavior of the experimental lift curve. With the failure of γ-Re_θ and forced transition, attempts at predicting transitional effects within this flow were

abandoned. These failures indicate that RANS CFD in the production codes used here is not well suited to predict transition characteristics for this type of flow.

Next, the effects of the upper and lower wind tunnel walls on the flow were examined. By comparing results from a free-air grid to results from structured tunnel grids, the tunnel walls in this experiment were determinrd to have a significant impact on the pressure distribution on the airfoil. To compare CFD results directly with the experimental data, the inclusion of upper and lower tunnel walls in computations is recommended.

Finally, the ability of 2-D RANS CFD to model the effects of slot blowing on the flow was evaluated. Results from this study indicate that CFD is capable of qualitatively capturing the blowing effects reasonably well. Lift coefficient and pressure distribution results from CFD matched fairly well with experimental values at low angles of attack ($\alpha < 5^\circ$, approximately). The lift curve nonlinear behavior was never captured, and C_L values maintained a mostly linear relationship with angle of attack up until the stall angle for each value of C_μ. Overall, the predicted stall angle for each C_μ was well in line with each stall angle in the experiment.

As expected, 2-D RANS struggled to accurately model the test cases involving highly separated flows. Flow solutions for these cases were poor, even when run time accurately. Stalled solutions obtained with time-accurate RANS runs appeared to be more sensitive to the choice of turbulence model, but neither model predicted surface pressure coefficients well in comparison with experiment. Generally, 2-D RANS is not advisable for use on test cases in which the airfoil has stalled and in which the flow exhibits massive separation.

Preliminary 3-D computations suggested the presence of noteworthy three-dimensional effects present in this experiment, particularly at high angles of attack, suggesting that 2-D CFD should generally be avoided for all but qualitative trend analysis. Several interesting flow features were identified. More 3-D CFD trials are necessary to better understand the full impact of these features on both the CFD and the experimental pressure data.

Overall, this experimental data set is a very challenging one for CFD. Many of its features—including transitional flow, low-aspect-ratio with three-dimensionality, and unsteady, massive separation—make 2-D steady RANS very unsuitable for its prediction, in a quantitative sense. Although the current mostly 2-D study (as well as another independent 2-D study referenced) was able to qualitatively capture the effects of different blowing rates on the lift, clearly the CFD results are quantitatively inaccurate, especially at higher angles of attack when significant separation is present. Future work should include more attempts with transition prediction models, as well as 3-D simulations with eddy-resolving (i.e., beyond RANS) capability. Also, the qualitative ability of RANS to capture trends for other data from this experiment should be assessed, including unsteady pitching, unsteady low frequency slot blowing, the combination of pitching and steady slot blowing, and the combination of pitching and surging with unsteady slot blowing.

References

1. Greenblatt, D., "Unsteady Low-Speed Wind Tunnels," *AIAA Journal*, Vol. 54, No. 6, 2016, pp. 1817–1830.

2. Muller-Vahl, H. F., Strangfeld, C., Nayeri, C. N., Paschereit, C. O., Greenblatt, D., "Control of Thick Airfoil, Deep Dynamic Stall Using Steady Blowing," *AIAA Journal*, Vol. 53, No. 2, 2015, pp. 277–295, doi: 10.2514/1.J053090.

3. Muller-Vahl, H. F., Nayeri, C. N., Paschereit, C. O., Greenblatt, D., "Dynamic Stall Control via Adaptive Blowing," *Renewable Energy*, Vol. 97, 2016, pp. 47–64.

4. Poisson-Quinton, P. and Lepage, L., "Boundary Layer and Flow Control: Its Principles and Application," Survey of French Research on the Control of Boundary Layer and Circulation, edited by Lachmann, G. V., Vol. 1, Pergamon, New York, 1961, pp. 21–73.

5. Krist, S. L., Biedron, R. T., and Rumsey, C. L., "CFL3D User's Manual (Version 5.0)," NASA-TM-208444, June 1998.

6. Roe, P. L., "Approximate Riemann Solvers, Parameter Vectors, and Difference Schemes," *Journal of Computational Physics*, Vol. 43, 1981, pp. 357–372.

7. Spalart, P. R. and Allmaras, S. R., "A One-Equation Turbulence Model for Aerodynamic Flows," *Recherche Aerospatiale*, No. 1, 1994, pp. 5–21.

8. Menter, F. R., "Two-Equation Eddy-Viscosity Turbulence Models for Engineering Applications," *AIAA Journal*, Vol. 32, No. 8, 1994, pp. 1598–1605.

9. Langtry, R. B. and Menter, F. R., "Correlation-Based Transition Modeling for Unstructured Parallelized Computational Fluid Dynamics Codes," *AIAA Journal*, Vol. 47, No. 12, 2009, pp. 2894–2906.

10. Rumsey, C. L., "Turbulence Modeling Resource," https://turbmodels.larc.nasa.gov, cited 11/15/2016.

11. Anderson, W. K. and Bonhaus, D. L., "An Implicit Upwind Algorithm for Computing Turbulent Flows on Unstructured Grids," *Computers and Fluids*, Vol. 23, No. 1, 1994, pp. 1–22.

12. Anderson, W. K., Rausch, R. D., and Bonhaus, D. L., "Implicit/Multigrid Algorithm for Incompressible Turbulent Flows on Unstructured Grids," AIAA Paper 95–1740–CP, 12th Computational Fluid Dynamics Conference, San Diego, CA, June, 1995.

13. Nielsen, E. J., Lu, J., Park, M. A., and Darmofal, D. L., "An Implicit, Exact Dual Adjoint Solution Method for Turbulent Flows on Unstructured Grids," *Computers and Fluids*, Vol. 33, No. 9, 2004, pp. 1131–1155.

14. Laufer, M., "CFD Predictions of Load Control Using Steady Blowing on a Thick Airfoil," Proceedings of 34th Israeli Conference of Mechanical Engineering, Haifa, November 2016.

15. Yamamoto, K., Tanaka, K., and Murayama, M., "Comparison Study of Drag Prediction for the 4th CFD Drag Prediction Workshop Using Structured and Unstructured Mesh Methods," AIAA Paper 2010-4222, June 2010.

16. Bordji, M., Gand, F., Deck, S., and Brunet, V., "Investigation of a Nonlinear Reynolds-Averaged Navier-Stokes Closure for Corner Flows," *AIAA Journal*, Vol. 54, No. 2, 2016, pp. 386–398.

17. Spalart, P. R., "Strategies for Turbulence Modelling and Simulations," *International Journal of Heat and Fluid Flow*, Vol. 21, 2000, pp. 252–263.

18. Shur, M. L., Strelets, M. K., Travin, A. K., and Spalart, P. R., "Turbulence Modeling in Rotating and Curved Channels: Assessing the Spalart-Shur Correction," *AIAA Journal*, Vol. 38, No. 5, 2000, pp. 784–792.

19. Rumsey, C. L., Lee-Rausch, E. M., Watson, R. D., "Three-Dimensional Effects in Multi-Element High Lift Computations," *Computers & Fluids*, Vol. 32, 2003, pp. 631–657.

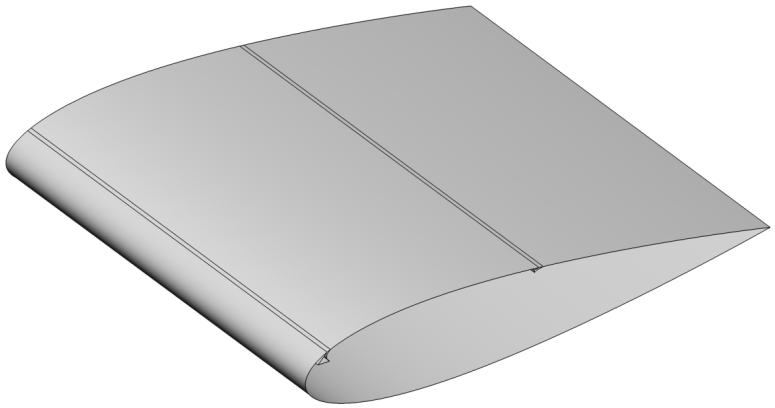

(a) Airfoil with slots

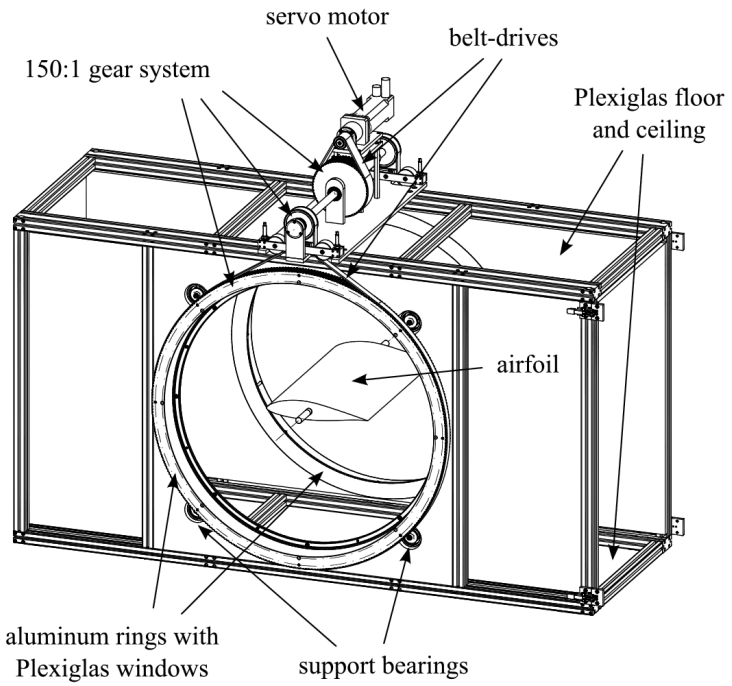

(b) Experimental setup for test cases [2]

Figure 1. Problem Geometry.

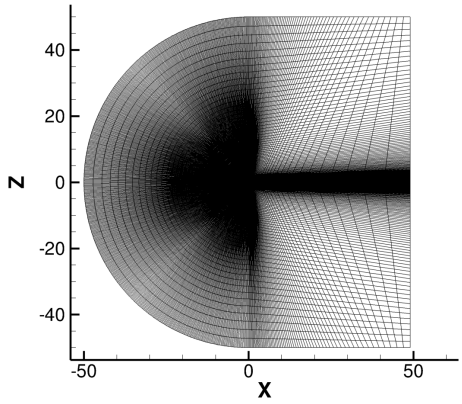

(a) 2-D, structured, free-air grid

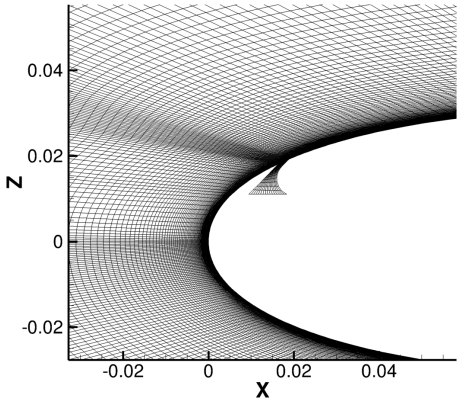

(b) 2-D, structured, free-air grid (close view)

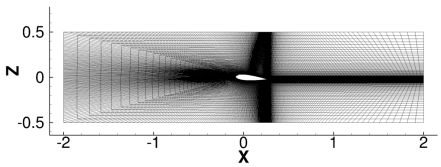

(c) 2-D, structured, tunnel grid

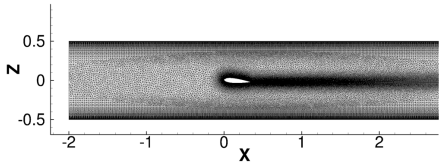

(d) 2-D, unstructured, tunnel grid

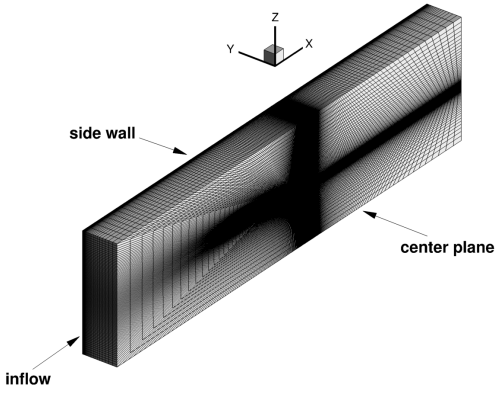

(e) 3-D, structured, tunnel grid

Figure 2. Examples of grids employed.

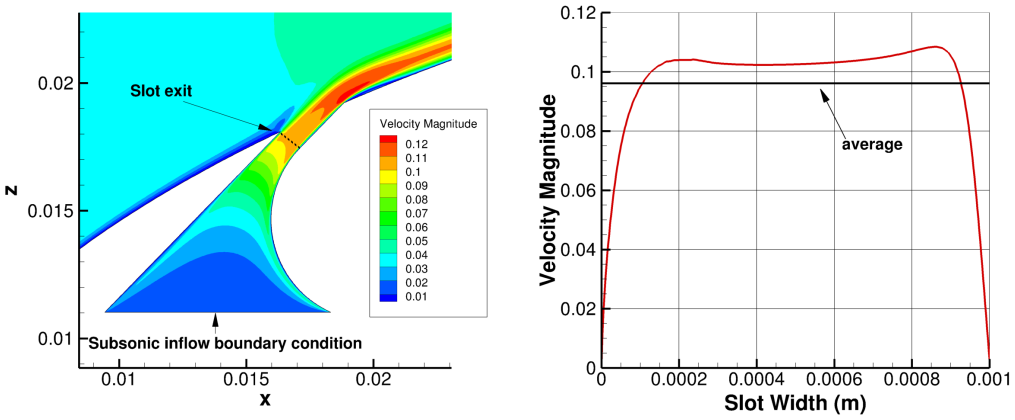

(a) Slot geometry

(b) Example slot velocity profile

Figure 3. Jet velocity was considered to be the average velocity magnitude across the slot exit line (velocity is nondimensionalized by a_{ref}).

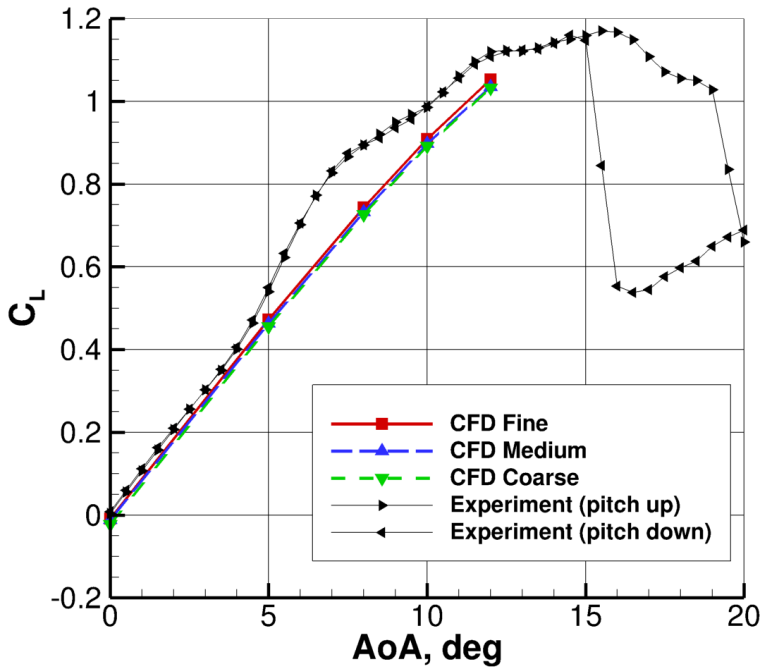

Figure 4. Grid sensitivity study for 2-D, structured, free-air grids, no blowing, FUN3D with SA model.

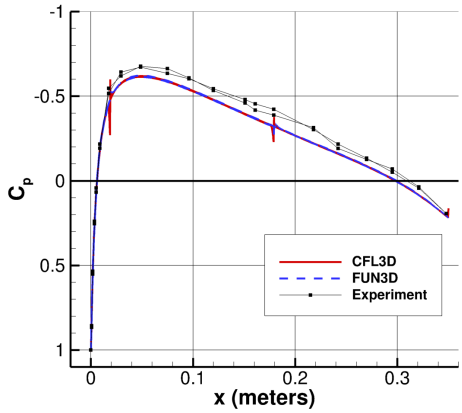

(a) $\alpha = 0^\circ$

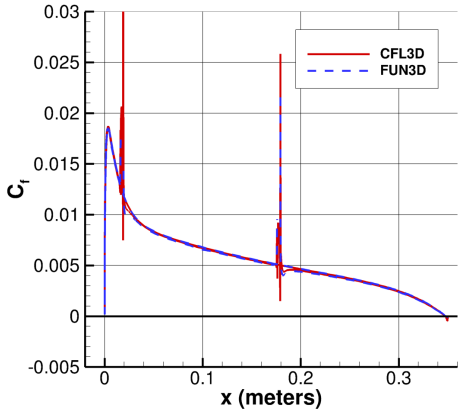

(b) $\alpha = 0^\circ$

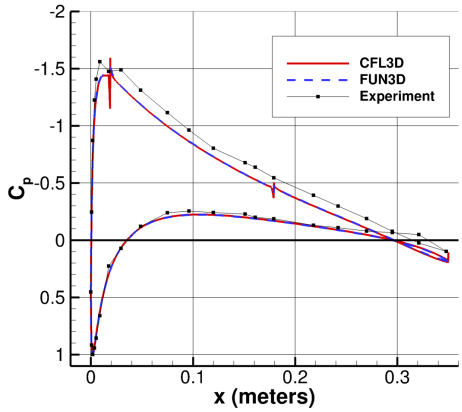

(c) $\alpha = 5^\circ$

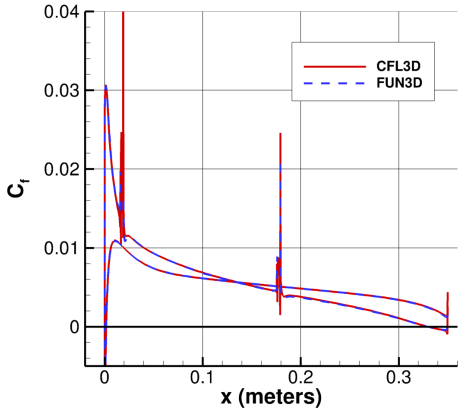

(d) $\alpha = 5^\circ$

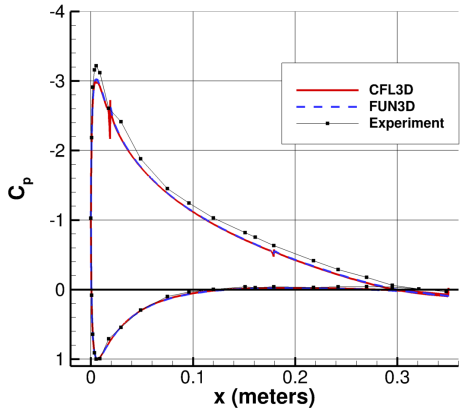

(e) $\alpha = 10^\circ$

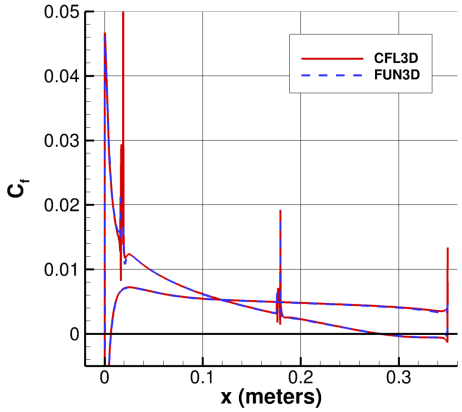

(f) $\alpha = 10^\circ$

Figure 5. Results from comparison cases between CFL3D and FUN3D, 2-D, structured, free-air grids, no blowing, with SA model.

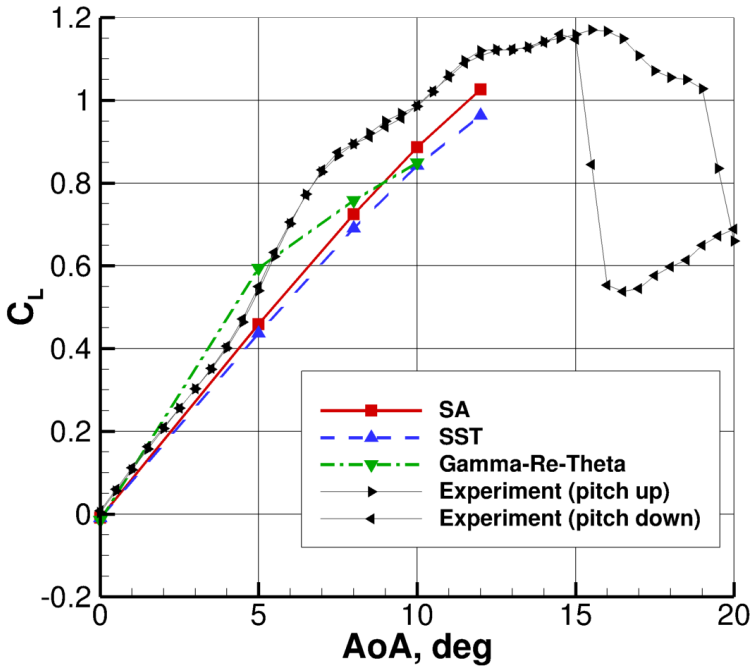

Figure 6. Comparison of lift coefficient results from the three different turbulence models, 2-D, structured, free-air grids, no blowing, CFL3D.

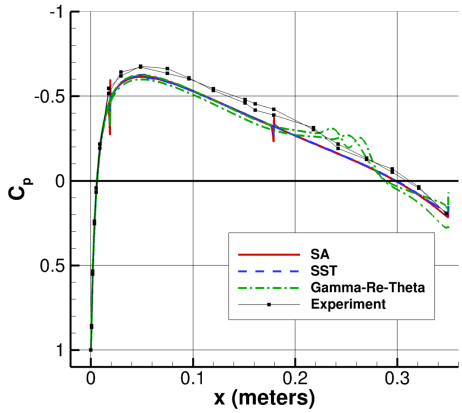

(a) $\alpha = 0^\circ$

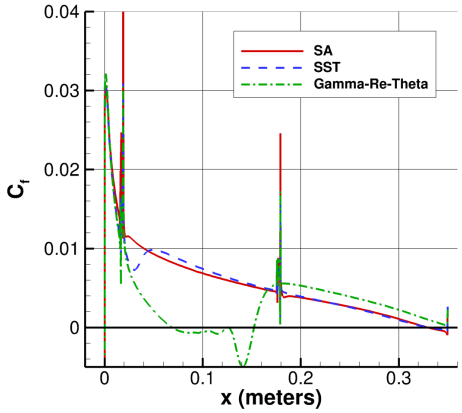

(b) $\alpha = 0^\circ$

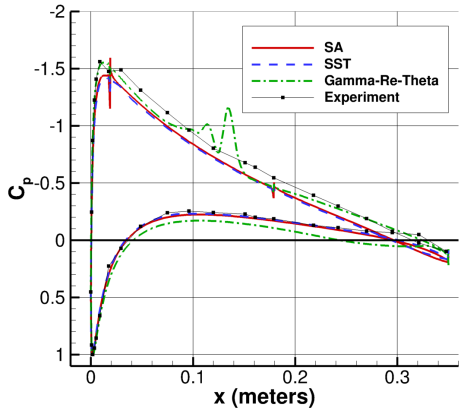

(c) $\alpha = 5^\circ$

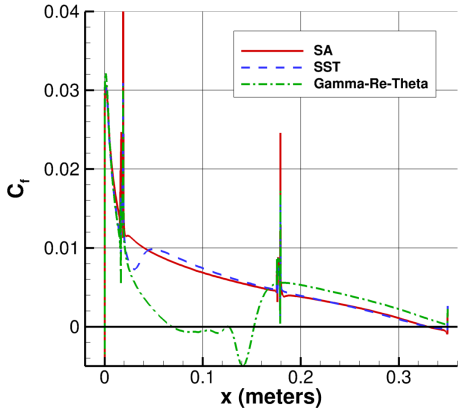

(d) $\alpha = 5^\circ$

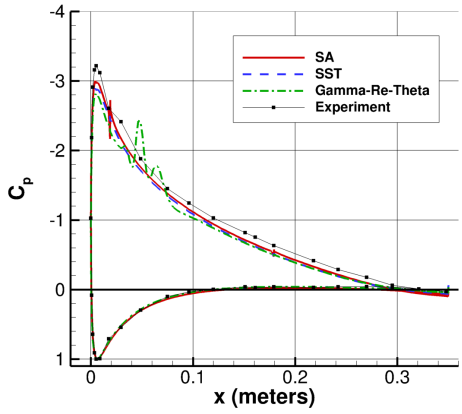

(e) $\alpha = 10^\circ$

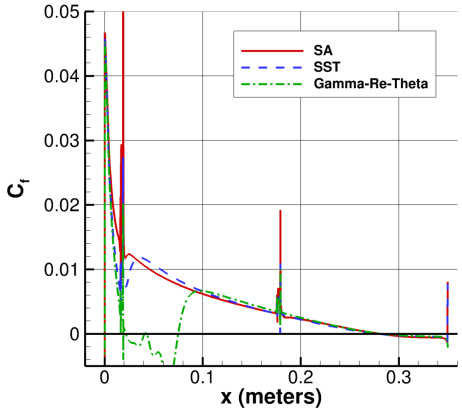

(f) $\alpha = 10^\circ$

Figure 7. Comparison of pressure and skin friction coefficient results from the three turbulence models, 2-D, structured, free-air grids, no blowing, CFL3D.

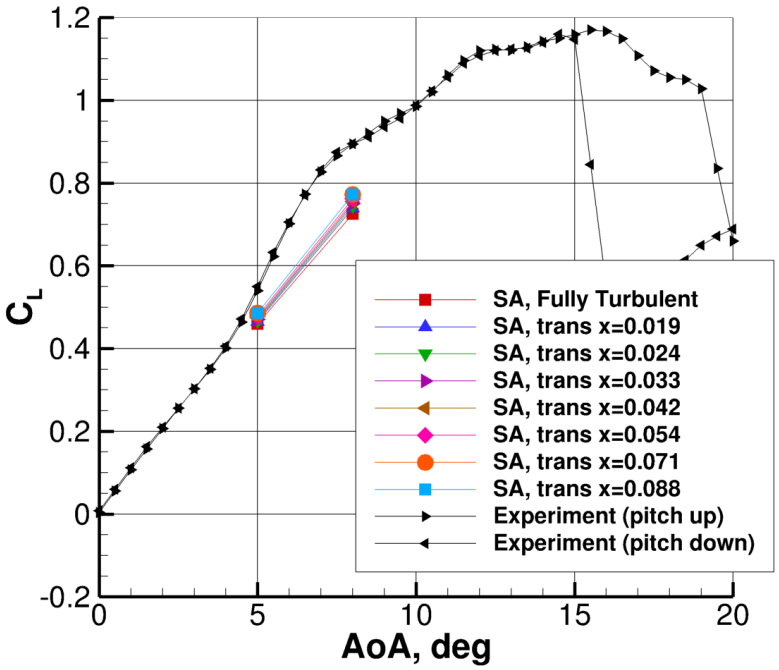

Figure 8. Lift coefficient results from the forced transition study, 2-D, structured, free-air grids, no blowing, CFL3D with SA model.

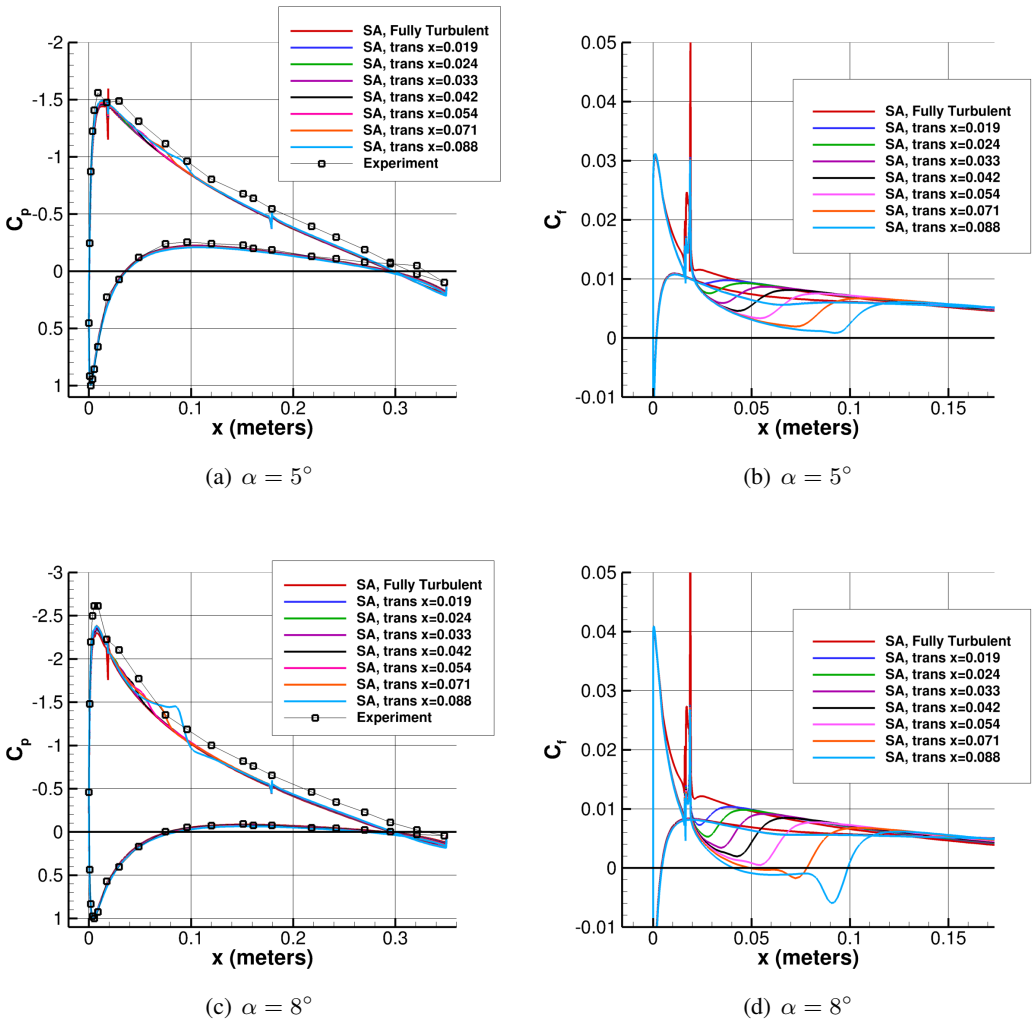

(a) $\alpha = 5^\circ$ (b) $\alpha = 5^\circ$

(c) $\alpha = 8^\circ$ (d) $\alpha = 8^\circ$

Figure 9. Pressure and skin friction coefficient results from the forced transition study, 2-D, structured, free-air grids, no blowing, CFL3D with SA model.

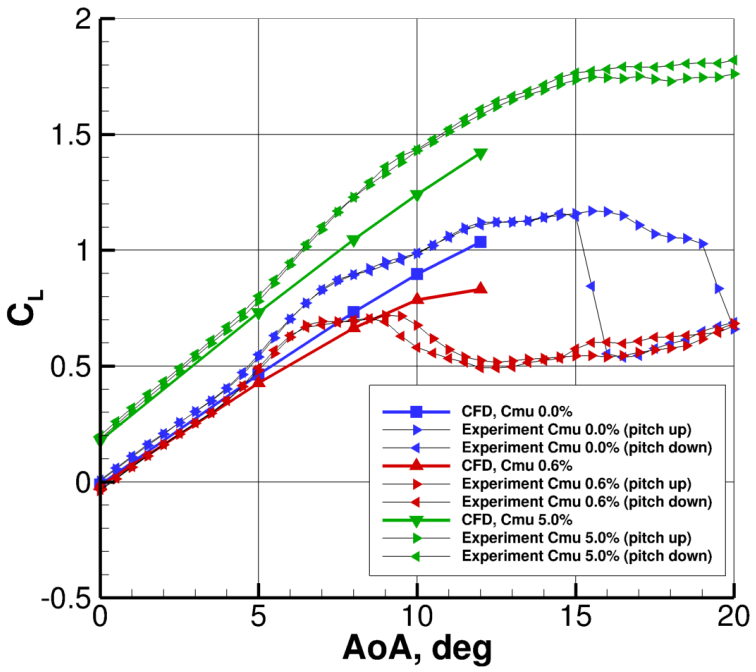

Figure 10. Lift coefficient results with slot blowing on a 2-D, structured, free-air grid, FUN3D with SA model.

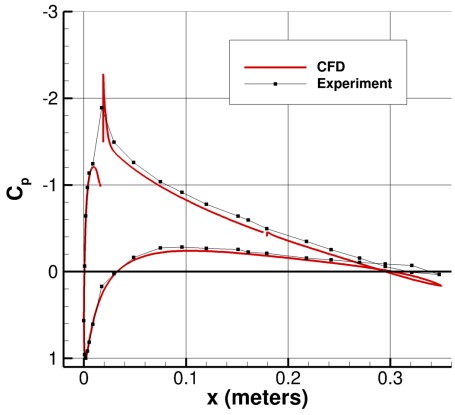

(a) $\alpha = 5°, C_\mu = 0.6\%$

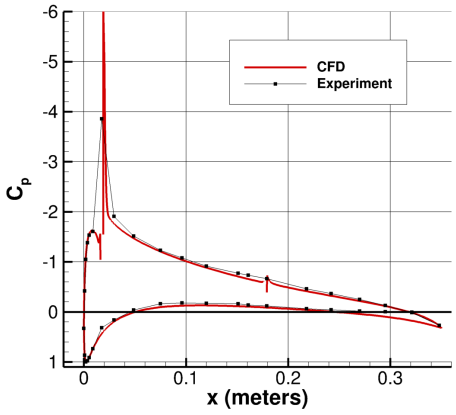

(b) $\alpha = 5°, C_\mu = 5.0\%$

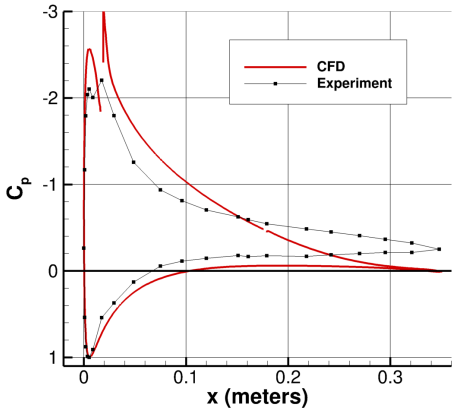

(c) $\alpha = 10°, C_\mu = 0.6\%$

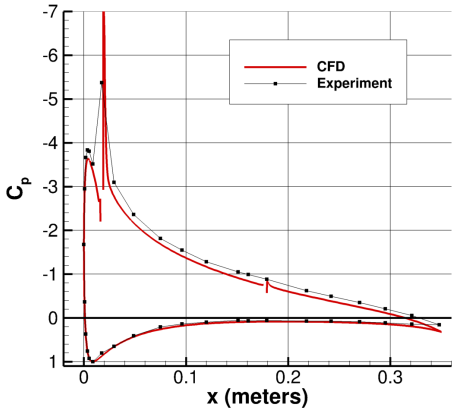

(d) $\alpha = 10°, C_\mu = 5.0\%$

Figure 11. Pressure distribution results with slot blowing on a 2-D, structured, free-air grid, FUN3D with SA model.

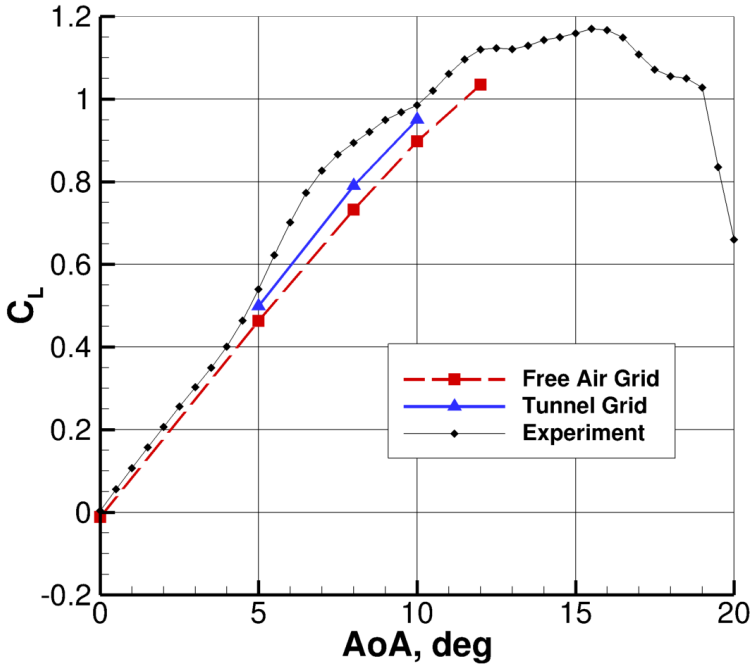

Figure 12. Comparison between lift coefficient results from a 2-D structured free-air grid and a 2-D structured tunnel grid, no blowing, FUN3D with SA model.

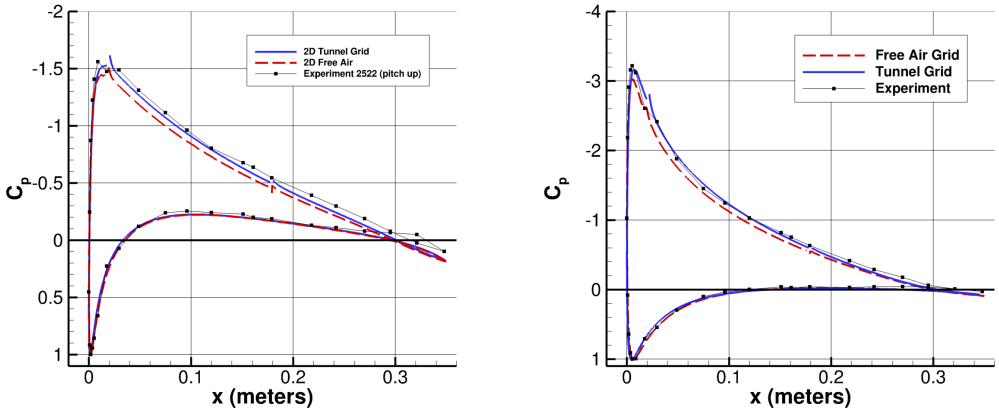

(a) $\alpha = 5^\circ$ (b) $\alpha = 10^\circ$

Figure 13. Comparison between pressure distribution results from a 2-D structured free-air grid and a 2-D structured tunnel grid, no blowing, FUN3D with SA model.

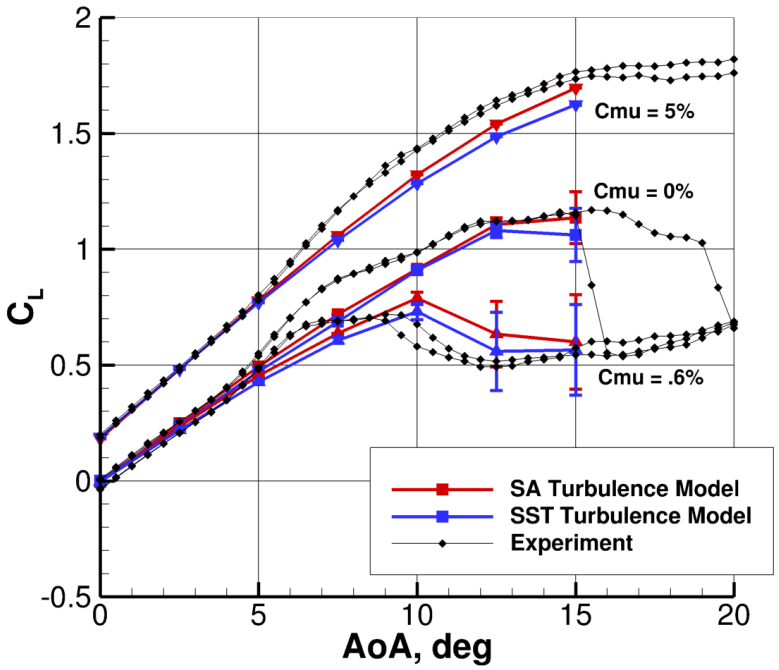

Figure 14. Lift coefficient results with slot blowing on a 2-D unstructured tunnel grid, FUN3D (run in steady-state mode).

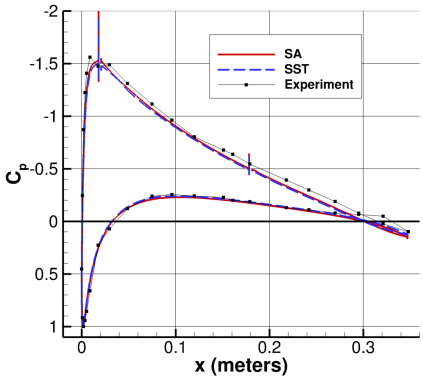

(a) $\alpha = 5^\circ, C_\mu = 0\%$

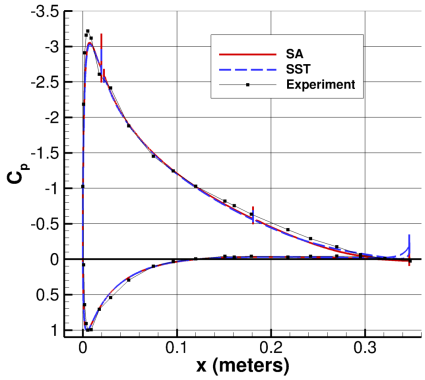

(b) $\alpha = 10^\circ, C_\mu = 0\%$

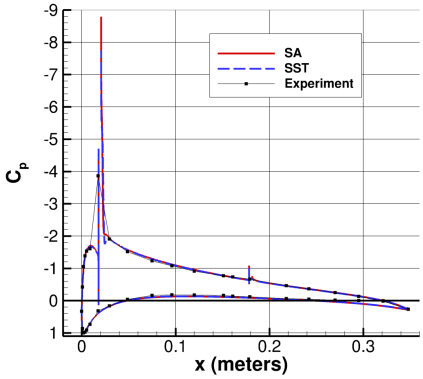

(c) $\alpha = 5^\circ, C_\mu = 5\%$

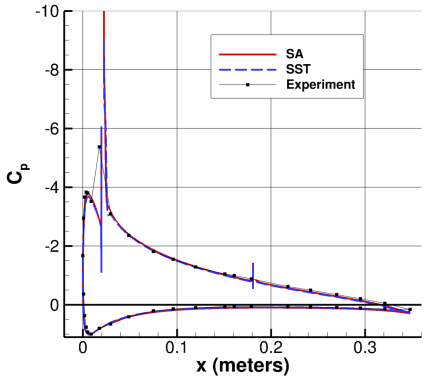

(d) $\alpha = 10^\circ, C_\mu = 5\%$

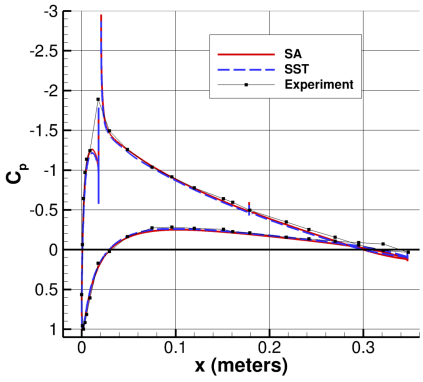

(e) $\alpha = 5^\circ, C_\mu = .6\%$

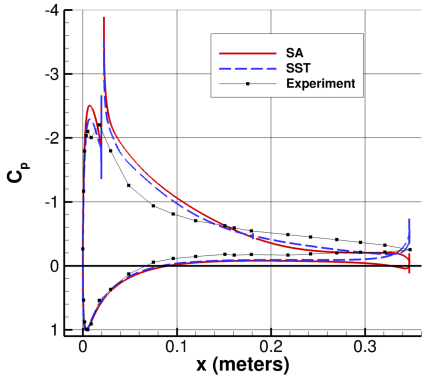

(f) $\alpha = 10^\circ, C_\mu = .6\%$

Figure 15. Pressure distribution results with slot blowing on a 2-D unstructured tunnel grid, FUN3D (run in steady-state mode); error bars represent the amplitude of oscillation in the solution.

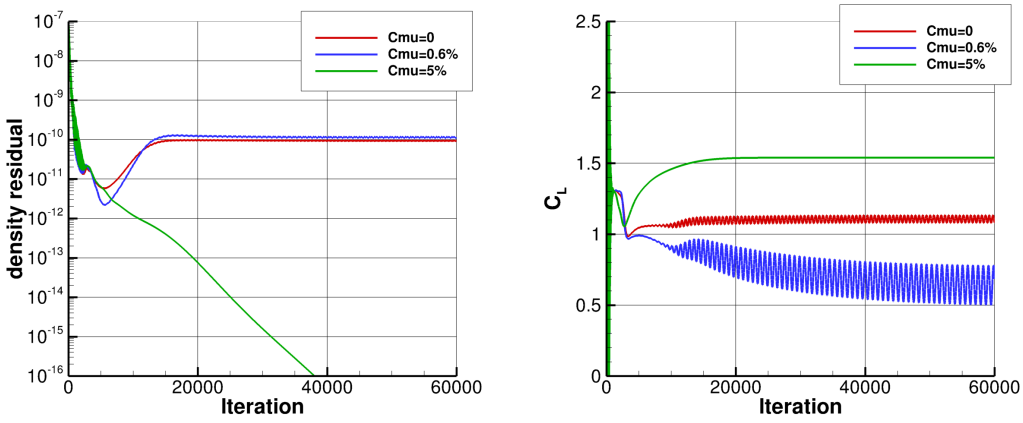

(a) Density residual (b) Lift coefficient

Figure 16. Iterative convergence histories from FUN3D for $\alpha = 12.5°$ on a 2-D unstructured tunnel grid, run in steady-state mode, SA model.

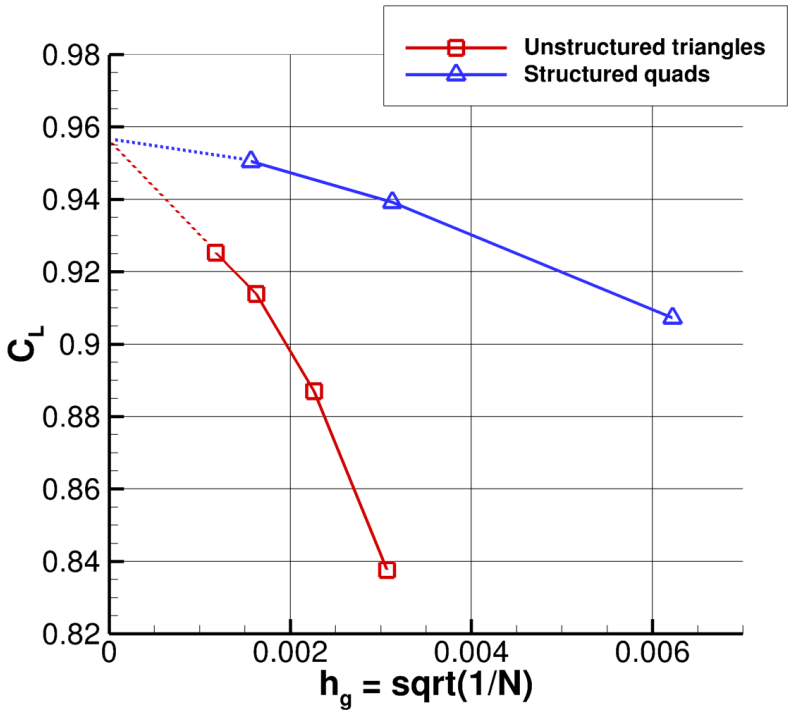

Figure 17. Grid convergence study using FUN3D on two different grid types; $\alpha = 10°$ in tunnel, SA model.

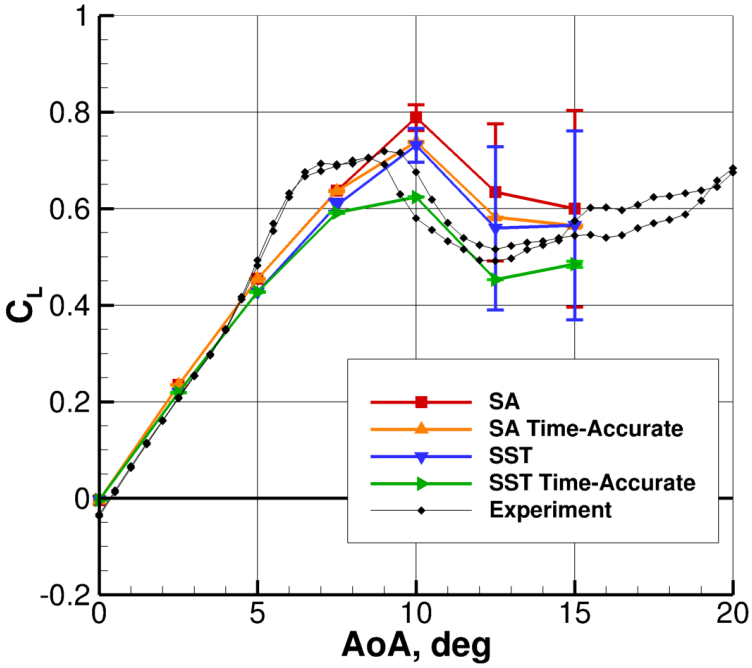

Figure 18. Comparison of time-accurate and steady solutions for $C_\mu = 0.6\%$ cases, 2-D unstructured tunnel grid, FUN3D; error bars represent the amplitude of oscillation in the solution.

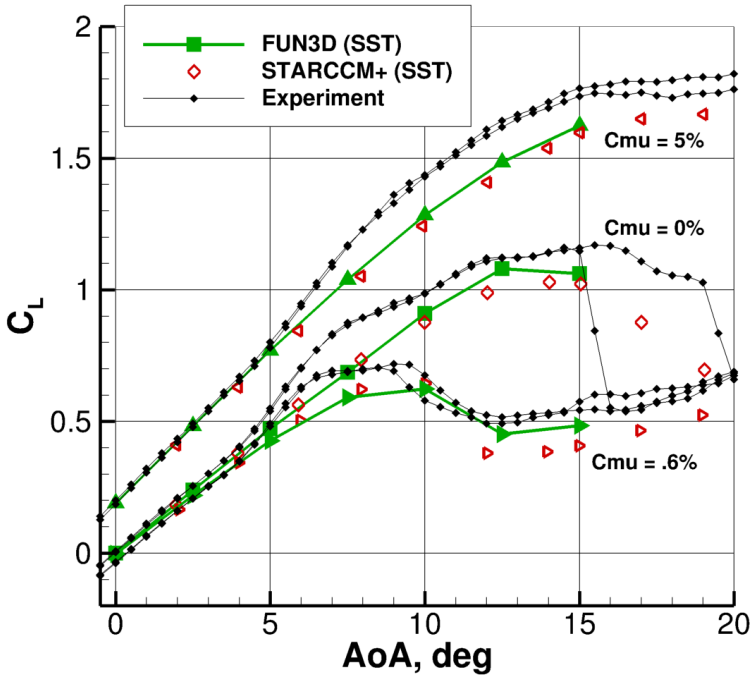

Figure 19. Comparison of current 2-D FUN3D SST solutions with SST solutions from STARCCM+ in Laufer [14].

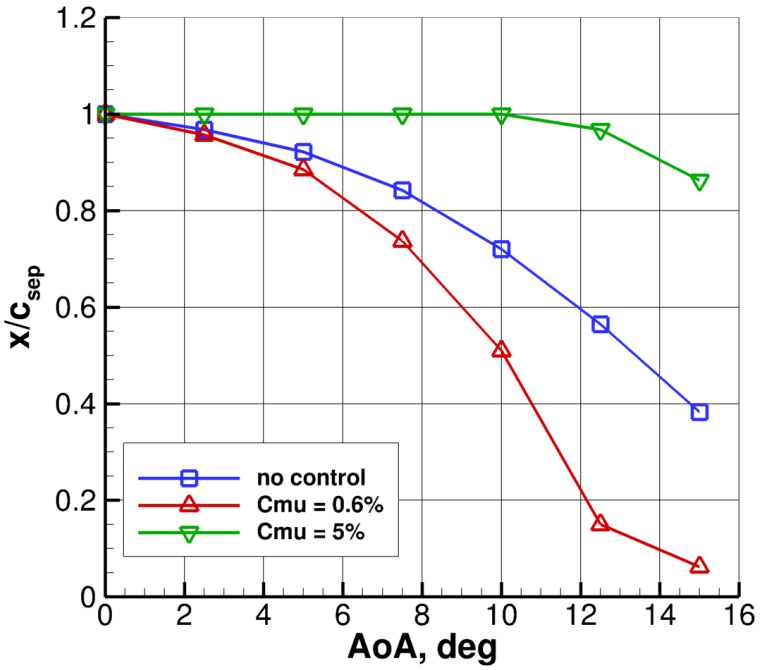

Figure 20. Effect of blowing on trailing edge separation location, 2-D unstructured tunnel grid, FUN3D with SA model.

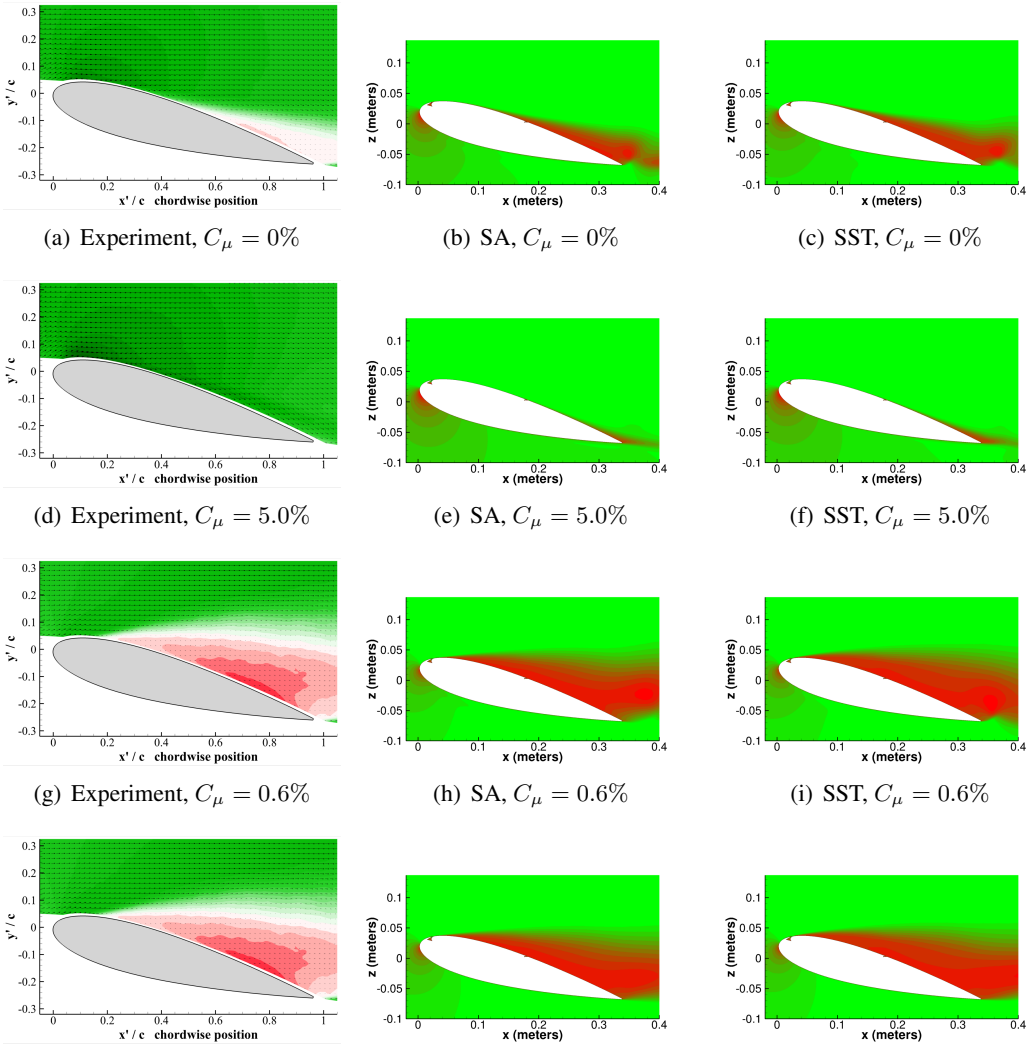

(a) Experiment, $C_\mu = 0\%$ (b) SA, $C_\mu = 0\%$ (c) SST, $C_\mu = 0\%$

(d) Experiment, $C_\mu = 5.0\%$ (e) SA, $C_\mu = 5.0\%$ (f) SST, $C_\mu = 5.0\%$

(g) Experiment, $C_\mu = 0.6\%$ (h) SA, $C_\mu = 0.6\%$ (i) SST, $C_\mu = 0.6\%$

(j) Experiment, $C_\mu = 0.6\%$ (k) Time-accurate SA, $C_\mu = 0.6\%$ (l) Time-accurate SST, $C_\mu = 0.6\%$

Figure 21. Velocity field results from FUN3D.

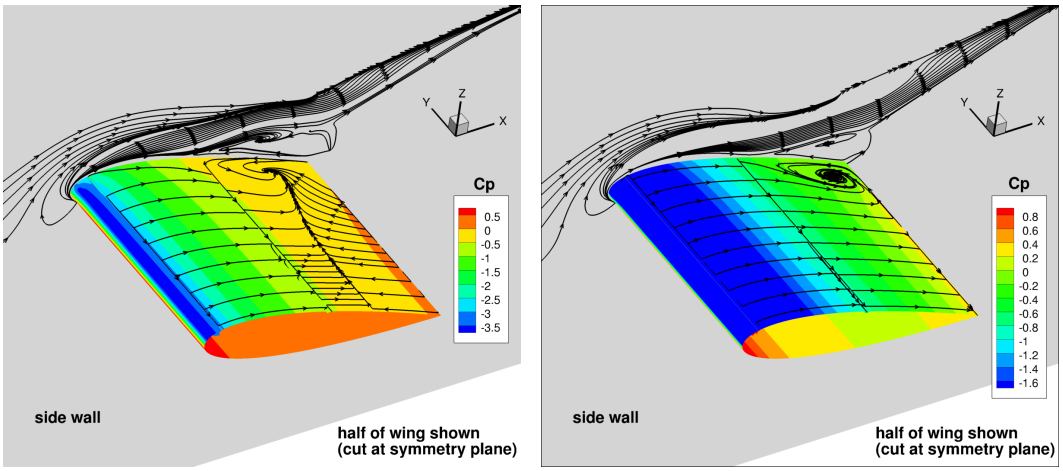

(a) $C_\mu = 0\%$ (b) $C_\mu = 5.0\%$

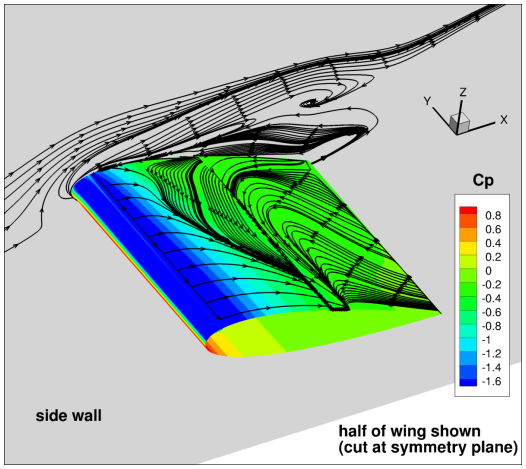

(c) $C_\mu = 0.6\%$

Figure 22. Initial 3-D results from CFL3D, displaying the effect that the juncture with the wind tunnel wall has on the overall flow; $\alpha = 12.5°$, 3-D structured grid with inviscid lower/upper walls, viscous side walls, SA model.

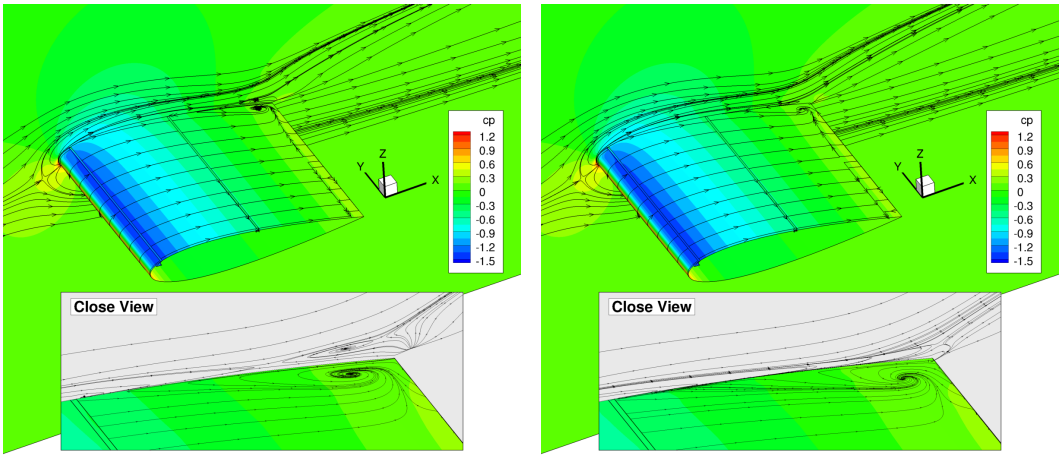

(a) SA model (b) SA-RC-QCR2000

Figure 23. Comparison of 3-D results from FUN3D with the SA turbulence model with and without Rotation/Curvature Correction (RC) and Quadratic Constitutive Relation (QCR2000); $\alpha = 5°$, $C_\mu = 0\%$, 3-D structured grid with inviscid lower/upper walls, viscous side walls.

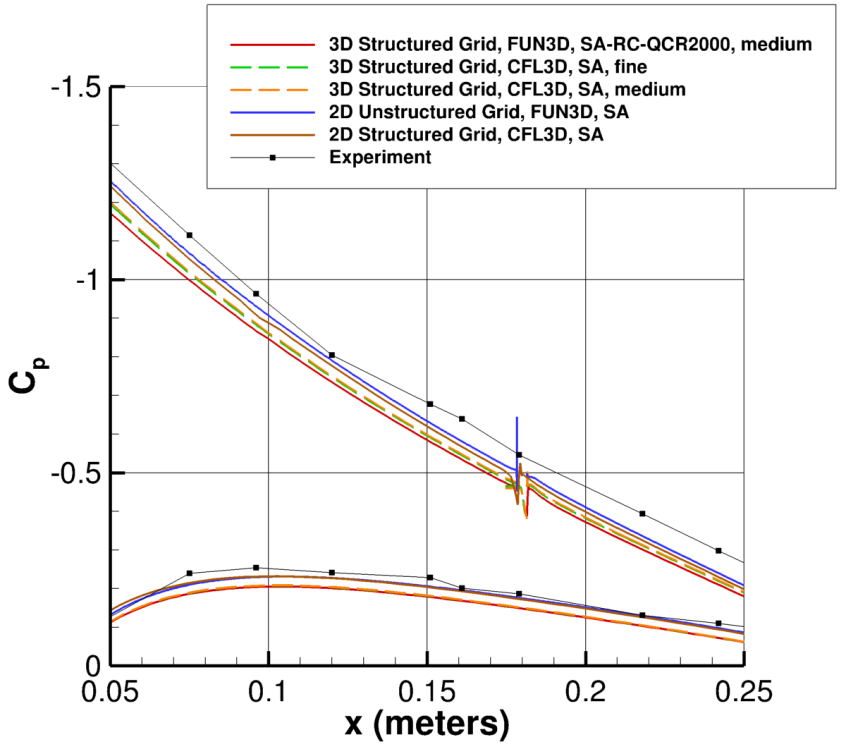

Figure 24. Zoomed comparison of 3-D surface pressure coefficients from FUN3D and CFL3D to 2-D results (all with tunnel walls) and experimental values, $\alpha = 5°$.

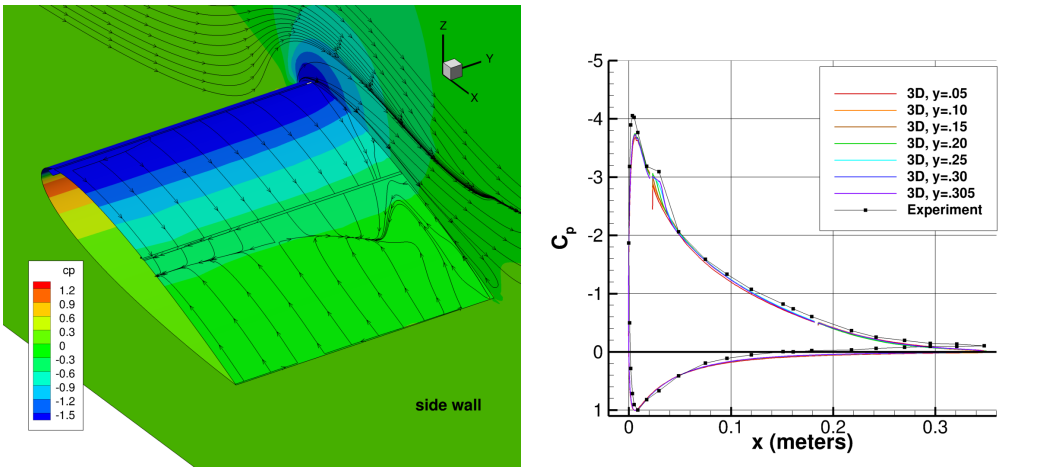

(a) Surface streamlines

(b) Surface pressure coefficients at cuts along the span

Figure 25. 3-D flow solution from FUN3D at $\alpha = 12.5°$, SA-RC-QCR2000.

REPORT DOCUMENTATION PAGE	Form Approved OMB No. 0704–0188

1. REPORT DATE *(DD-MM-YYYY)*	2. REPORT TYPE	3. DATES COVERED *(From - To)*
01-04-2017	Technical Memorandum	

4. TITLE AND SUBTITLE
CFD Study of NACA 0018 Airfoil with Flow Control

5a. CONTRACT NUMBER

5b. GRANT NUMBER

5c. PROGRAM ELEMENT NUMBER

6. AUTHOR(S)
Eggert, Christopher A.; Rumsey, Christopher L.

5d. PROJECT NUMBER

5e. TASK NUMBER

5f. WORK UNIT NUMBER
109492.02.07.01.01

7. PERFORMING ORGANIZATION NAME(S) AND ADDRESS(ES)
NASA Langley Research Center
Hampton, Virginia 23681-2199

8. PERFORMING ORGANIZATION REPORT NUMBER
L–20799

9. SPONSORING/MONITORING AGENCY NAME(S) AND ADDRESS(ES)
National Aeronautics and Space Administration
Washington, DC 20546-0001

10. SPONSOR/MONITOR'S ACRONYM(S)
NASA

11. SPONSOR/MONITOR'S REPORT NUMBER(S)
NASA/TM–2017–219602

12. DISTRIBUTION/AVAILABILITY STATEMENT
Unclassified-Unlimited
Subject Category 02
Availability: NASA STI Program (757) 864-9658

13. SUPPLEMENTARY NOTES
An electronic version can be found at http://ntrs.nasa.gov.

14. ABSTRACT

The abilities of two different Reynolds-Averaged Navier-Stokes codes to predict the effects of an active flow control device are evaluated. The flow control device consists of a blowing slot located on the upper surface of an NACA 0018 airfoil, near the leading edge. A second blowing slot present on the airfoil near mid-chord is not evaluated here. Experimental results from a wind tunnel test show that a slot blowing with high momentum coefficient will increase the lift of the airfoil (compared to no blowing) and delay flow separation. A slot with low momentum coefficient will decrease the lift and induce separation even at low angles of attack. Two codes, CFL3D and FUN3D, are used in two-dimensional computations along with several different turbulence models. Two of these produced reasonable results for this flow, when run fully turbulent. A more advanced transition model failed to predict reasonable results, but warrants further study using different inputs. Including inviscid upper and lower tunnel walls in the simulations was found to be important in obtaining pressure distributions and lift coefficients that best matched experimental data. A limited number of three-dimensional computations were also performed.

15. SUBJECT TERMS
CFD, flow control

16. SECURITY CLASSIFICATION OF:			17. LIMITATION OF ABSTRACT	18. NUMBER OF PAGES	19a. NAME OF RESPONSIBLE PERSON
a. REPORT	b. ABSTRACT	c. THIS PAGE			STI Information Desk (help@sti.nasa.gov)
U	U	U	UU	39	19b. TELEPHONE NUMBER *(Include area code)* (757) 864-9658